United States
Department of
Agriculture

Forest Service

**Intermountain
Forest and Range
Experiment Station
Ogden, Utah 84401**

Research
Paper INT-309

April 1983

Potential Spotting Distance from Wind-Driven Surface Fires

Frank A. Albini

THE AUTHOR

FRANK A. ALBINI is a mechanical engineer, assigned to the Fire Fundamentals research work unit at the Northern Forest Fire Laboratory in Missoula, Mont. He earned a Ph.D. from the California Institute of Technology in 1962, where he also obtained his undergraduate training (B.S. 1958, M.S. 1959). He joined the Forest Service in October 1973 after 12 years of pure and applied research and systems analysis both in private industry and at the nonprofit Institute for Defense Analyses.

RESEARCH SUMMARY

This paper documents a speculative model of the process by which firebrand particles are lofted into the air through the action of buoyancy-induced airflow near the head of a wind-driven fire in surface fuels. It is postulated that the particles are lofted by strong thermals generated by the fire. The fire and the thermals it generates are idealized as being two-dimensional, for analytical tractability. It is further postulated that the fire generates the thermals because the intensity of the fire fluctuates with time in response to variations in windspeed or "gustiness." An increase in intensity above the average value, sustained for some period of time, is assumed to give birth to a line thermal with energy/length (or "strength") equal to the excess energy/length afforded by the intensity excursion. The author has previously published theoretical power spectral densities of intensity variations of line fires in typical wildland fuels, based on a model for the dynamic response of the fire to windspeed variations and an empirical power spectrum function for horizontal wind gustiness near the surface. A simple stochastic sequence of excursions of intensity is used as a surrogate process to approximate these power spectra and so allow explicit expression of thermal strength as a function of windspeed, mean fire intensity, and fuel type. The trajectories of particles lofted by line thermals have been described elsewhere by the author. Maximum viable firebrand height was shown to be proportional to the square root of the thermal strength, and the downwind drift distance during lofting proportional to the product of windspeed and the square root of the loft height. The equations for predicting maximum firebrand height and drift distance during lofting are summarized here in simple form for easy field use. Once the maximum viable firebrand height is known, it can be used to predict the distance downwind that the particle will travel before it returns to the ground. Equations for this calculation have been published elsewhere, and are available as pocket calculator programs. Because several elements of the model process are both speculative and not subject to direct validation, these results are to be considered tentative. Field tests of the spotting distance predictions are sought as a means of testing the utility of the model.

CONTENTS

Potential Spotting Distance from Wind-Driven Surface Fires

Frank A. Albini

INTRODUCTION

The spread of wildland fire by windborne sparks or embers, known as "spotting" in the vernacular of fire control, frequently frustrates fire suppression efforts. Since there is usually no practical preventive counter to spotting, timely prediction of the maximum distance over which spotting can be expected ahead of a fire front can be a valuable aid to tactical fire suppression planning. This paper addresses the problem of predicting the maximum spotting distance ahead of a wind-driven fire in surface fuels and presents a model for a process leading to intermediate-range spotting.

Fires burning under standing timber seldom cause spot fires at any significant distance unless the trees of the overstory become involved in the fire. This is so because the overstory crown layer affords a mechanical barrier that can intercept entrained firebrands and also interferes with development of a strong updraft that can lift firebrand particles. But when a tree, or a small group of trees, is ignited by the understory fire, it can burn briefly and vigorously. This event, called "torching," produces a strong transitory convective flow that can loft firebrand particles to significant heights. The lofting of firebrands by this mechanism and their subsequent transport by the ambient windfield have been modeled (Albini 1979). The model was extended (Albini 1981a) to include the lofting of firebrands by large, steady, isolated flames such as those from the burning of heavy fuel accumulations. The model and its extensions have been coded as algorithms for pocket calculators (Chase 1981) for easy field application.

A wind-driven fire in surface fuels without timber cover can give rise to significant spotting. Generally, the greater the intensity of the fire, the more severe the spotting problem it causes (Brown and Davis 1973; Luke and McArthur 1978). No quantitative model of the spotting distance from a spreading surface fire has been developed, although much of the phenomenology is widely known. The reason for this deficiency is that the fluid mechanical description of the interaction of wind and fire is both complex and singularly difficult to approximate with realism.

A model is presented here for intermediate-range spotting in which a spreading surface fire, idealized as a straight line perpendicular to the direction of the wind, provides the source of buoyancy that lofts firebrand particles above the ground for transport downwind. Short-range spotting of a few tens of meters from fires of low intensity is not addressed. Also not addressed is the very long-range spotting of tens of kilometers associated with severe fire phenomena such as the establishment of fire whirls or sustained spread of fire through the crowns of timber stands. These unique phenomena require separate treatments.

Not considered in this model is the probability that there exists a firebrand particle in the fuel complex that has the particular size that will permit it to be a maximum-distance spot fire source. Particles that are too small can be lofted to a greater height than that of the maximum-distance particle, but they will burn out before returning to the ground. Larger particles cannot be lofted so high, and thus will not travel as far. The probability of ignition by a firebrand particle is also not addressed in this paper. What is predicted is the distance to which a viable firebrand could be carried. If it fails to land upon a suitable fuel to ignite, or if the fire ignited fails to spread, no spot fire will occur.

The analysis presented here consists of several steps. Each step involves idealization and untestable approximation of the physical realities of the situation addressed. This oblique approach stems from the need to simplify the problem in order to deal with it analytically. But in making simplifying mathematical assumptions, one always faces the possibility of discarding or badly distorting important features of the physical situation. Because it is impossible to test some key approximations of the model presented here, it is important that they be documented because they are possible sources of error. By testing the predictions of the model against experience in the field, deficiencies can be discovered. Then further research can trace such defects to their sources within the model so they can be corrected. A major purpose of this paper, therefore, is to leave a well-marked trail through the analytical thicket of the model to help in finding and fixing the flaws it probably includes.

FORMULATION AND IDEALIZATION

In earlier works (Albini 1979, 1981a; Chase 1981), the trajectories of firebrand particles have been calculated, leading to formulae for spotting distance once the initial height of the particle is known. These formulae can be used to predict spotting distances from wind-aided free-burning fires in surface fuels as well. What remains to be done is to predict the maximum height of firebrand particles lofted by such fires using observable or calculable features of the behavior of the fire. As before, we consider only firebrand particles that have no aerodynamic lift (i.e., can not glide), so once the flow field of the hot plume above the fire is known, the lofting flight of an entrained particle can be calculated.

Thus the problem is reduced to that of describing the aerodynamic environment above a wind-aided surface fire. To model this flow field, it is necessary to simplify the description of the fire, because an oblong, growing fire perimeter, with intensity a function of position, is far too complex to use as a boundary condition in the fluid flow equations. The means of simplification chosen here is to describe only the most intense segment of the fire perimeter, its leading edge, and to treat this segment as a straight line perpendicular to the direction of the wind.

Wildland fires seldom, if ever, have shapes that closely resemble straight lines at their leading edges. Nevertheless the front of a wind-driven surface fire frequently is nearly perpendicular to the direction of the wind over a distance that is much larger than the extent of the burning zone in the direction of the wind. Focusing on this portion of the fire, where its intensity--as measured by the energy release rate per unit length of fire edge--is greatest, the front can be approximated as a straight line perpendicular to the direction of the wind. A mathematical idealization of this portion of the fire perimeter is that it extends indefinitely far in either direction. This is the conceptual line fire that is modeled here. The intention is to model a fire that, if it did exist, would produce an aerodynamic environment for firebrand particles that would closely mimic that which exists above the leading edge of a real fire.

The mathematically ideal line fire is a two-dimensional construct that does not exist, but can be closely approximated in laboratory simulations. By eliminating the third dimension from the problem, analysis is greatly simplified, and models of the ideal process can be assembled

and tested in the laboratory. This procedure has been widely followed in the field of fluid mechanics dealing with buoyancy-induced flows such as from fires or other sources of heat (Rouse 1947; Rankine 1950; Rouse, Yih, and Humphreys 1952; Priestly and Ball 1955; Lee and Emmons 1961; Putnam 1965; Gostintsev and Sukhanov 1977, 1978; Luti 1980, 1981; Albini 1981b, 1982; Fernandez-Pello and Mao 1981) or from the discharge of buoyant fluid from a line source (Scorer 1959; Richards 1963; Cederwall 1971; Roberts 1977, 1979a,b, 1980; Strobel and Chen 1980). Much can be learned from the study of such idealized approximations of the real world. If the essence of the physical process is captured, then scaling from the laboratory to the field, using mathematical modeling, can be done with confidence.

A relevant example of such scaling is the behavior of the buoyant plume from a line source in cross flow. Smoke from a heading or backing line fire in a wind is transported and dispersed by such a plume. Rankine (1950) reported experimental work done during World War II on the dispersal of fog over airport runways by a linear array of burners. The vertical and horizontal extent of the hot gas zone, as transported by a crossing wind, was to be scaled to the field situation from small indoor experiments. By dimensional analysis, he, Rouse (1947), and Taylor (1961) deduced the importance of the ratio of the cube of the windspeed to the heat source intensity as a determining factor in fixing the angle of the buoyant flow. Byram (1959) introduced this parameter to the characterization of forest fire behavior as a measure of the power of the wind relative to that of the fire. Putnam (1965) correlated flame tilt angle to a variable that Albini (1981b) showed to be the same as this ratio. In related research, Cederwall (1971) showed the influence of this parameter on the pattern of dispersal of buoyant effluent from a slot orifice under water. Roberts (1979a) showed experimentally that whether or not the plume from a finite-length line source in a cross flow detaches from the surface or is trapped against it depends solely on this ratio. Van Wagner (1973) used this parameter in his experimental correlation of fire intensity, windspeed, and tree crown scorch. Theoretical analysis of the buoyant plume from a line fire in wind (Gostintsev and Sukhanov 1977, 1978) showed that this ratio should have a dominant influence on plume geometry on a scale of tens of kilometers in the atmosphere. Recent numerical simulations (Luti 1980, 1981) suggest that this indeed may be so.

Using the experimental findings of Roberts (1979a), one can calculate the intensity at which a line fire should generate a plume that separates itself from the surface and rises as a distinct structure. This relationship is given in (1) and graphed in figure 1. This figure shows that fires in natural fuels should exhibit the entire range of plume behaviors, from standing to trapped against the surface in the nature of a boundary layer:

$$I = 17.5U^3 \qquad (1)$$

where I is minimum fire intensity (kW/m) and U is windspeed (m/s). Of course, this interpretation of the meaning of Roberts' experiments in terms of the behavior of fire plumes is subject to qualifications and cautions about applicability. The experiments were carried out in a free-surface water tunnel apparatus and the cross flow stream had a minimal level of turbulence. Furthermore, the velocity of the cross flow in the experiments was constant with height. All of these conditions are obviously violated by a free-burning fire. The analytical description of Gostintsev and Sukhanov (1977) showed the velocity profile with height to have a strong influence on plume geometry in the idealized two-dimensional case. So while the general behavior of a fire plume should be described qualitatively by the relationship graphed in figure 1, it should not be taken as definitive.

Armed with the prediction of figure 1, showing the general character of the flow field, one might consider modeling the mean flow structure of the plume using the integral method (Gostintsev and Sukhanov 1977, 1978). Were it not for the fact that the mean flow field should be expected to change character abruptly as the relationship between windspeed and fire intensity changes, such a model would be adequate. Because both windspeed (Davenport 1961; Doran and Powell 1982) and fire intensity (Albini 1983a) vary with time, the character of the mean flow field must be expected to alternate between plume and boundary layer types.

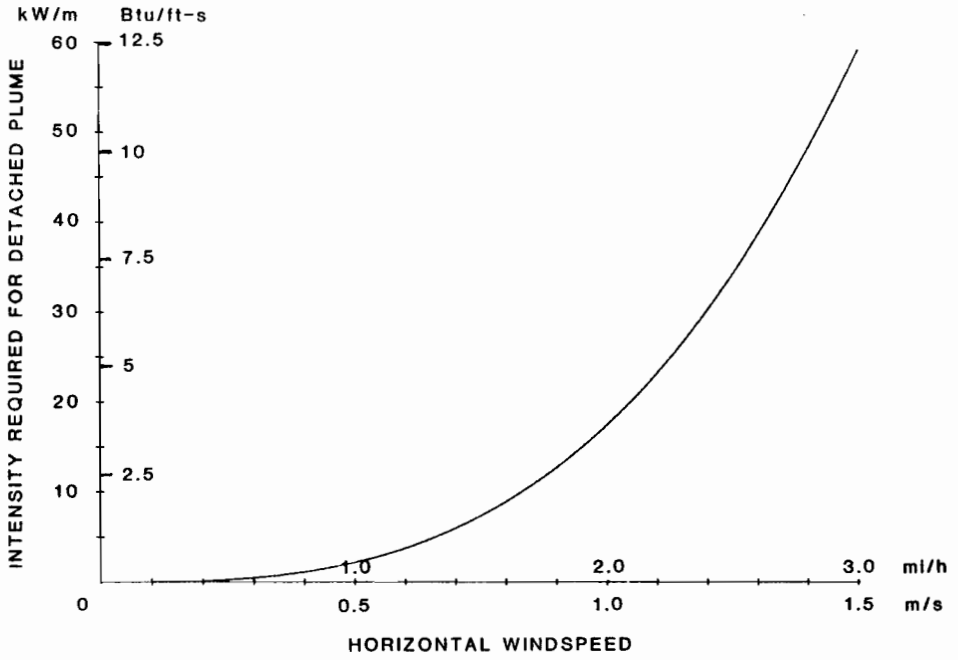

Figure 1.--Minimum fire intensity needed to produce a plume that separates from the surface as a distinct structure. The range of values is readily extended. If the windspeed is read as ten times the value on the horizontal axis of the graph, the intensity value read from the vertical axis is multiplied by 1,000. Read inner scales or outer scales on each axis, but do not mix them or readings will be incorrect.

TRANSPORT OF FIREBRAND PARTICLES BY THERMALS

The variation of fire intensity with time provides a mechanism for the generation of a sequence of puffs of buoyant fluid, called "thermals." This can occur as follows: When the intensity of the fire decreases to below average, as it should just after having been above average (Albini 1982), the plume tilts to an angle greater than average. This sequential alteration in the pattern of flow produces a "fold" in the plume sheet, like a wrinkle in a piece of fabric. This fold tends to pinch off and break away from the rest of the plume flow and rise as an isolated, coherent structure.

Thermals so generated are assumed in this model to provide the principal means of transporting firebrand particles. This hypothesis, crucial in the model's development, is unlikely ever to be tested directly. But if testing model predictions against experience in the field shows the predictions to be inaccurate, this assumption may be responsible.

The ability of a line thermal to transport firebrand particles has been analyzed (Albini 1983b), and the results are surprisingly simple in form. The maximum firebrand lofting height was found to be roughly proportional to the square root of the energy per unit length (or "strength") of the thermal. Equation (2) gives this relationship :

$$H = 0.173E^{1/2} \qquad (2)$$

where H is maximum firebrand height (m) and E is thermal strength (kJ/m).

When the particle exits the rising thermal, it will be some distance downwind from the fire front where the thermal originated. This additional travel distance must be added to the spotting distance predicted from the maximum firebrand height (Chase 1981). This added distance depends upon the profile of windspeed with height (Albini 1983b). If the windspeed varies as the seventh root of the height above ground (Plate 1971; Monteith 1973), then equation (3) should be used to calculate the downwind drift distance:

$$X = 2.78\ U(H)\ H^{1/2} \qquad (3)$$

where X is downwind drift distance (m) and U(H) is mean windspeed (m/s) at height H, which obeys the equation

$$U(H) = U(Z)(H/Z)^{1/7}, \qquad (4)$$

up to several hundred meters height (Plate 1971). Here Z is any convenient reference height (m) in the applicable range.

If the windspeed follows the logarithmic law of the wall (Monteith 1973), then equation (5) should be used:

$$X = 2.73\ U(h)\ H^{1/2}[2.13 + \ln(H/h)] \qquad (5)$$

where X is downwind drift distance (m), and U(h) is mean windspeed (m/s) at vegetation cover height h (m). This form may overestimate the windspeed for small values of h, in which case (3) should be used (Albini 1981a).

With these results, the modeling problem is reduced to that of predicting the strength of the thermals generated by a line fire.

STRENGTH OF THERMALS FROM A LINE FIRE

The conceptual process for generation of thermals described above relates the variation of fire intensity with time to the generation of thermals by a wind-driven surface line fire. The variation of fire intensity with time is caused by the variations in windspeed that are always present in the near-surface atmosphere (Davenport 1961; Doran and Powell 1982). A model for the response of a line fire to nonsteady wind (Albini 1982) was used with an empirical description of the variability--or gustiness--of the wind (Davenport 1961) to derive a general picture of the variations in fire intensity to be expected in different fuels (Albini 1983a). The variations of intensity are described in terms of the power spectral density of the sequence of deviations from the mean that each fuel type should exhibit.

Figures 2-4 show the power spectral densities of fire intensity variations for twelve of the thirteen stylized fuel models (Albini 1976) used for predicting wildfire behavior (Rothermel 1983). These figures were calculated as in Albini (1983a). The fuel types shown are those that are either ordinarily found without timber cover or are used to represent such. The model for closed timber litter (fuel model 8) has been omitted, but the model for hardwood litter (model 9) is included with the grass types in figure 2, since it is often used when the deciduous overstory is bare of leaves. The timber litter and understory type (model 10) is sometimes used to represent timber harvest debris that has become overgrown with shrubs or other surface vegetation, so it is included with the logging slash fuel models in figure 3. The shrub fuel types are grouped together in figure 4. In each of these figures, the windspeed is shown in the upper righthand corner of each panel. This windspeed is the mean--long term average--value of the horizontal windspeed measured at the international anemometer standard height of ten meters above the ground.

These figures illustrate that there is very little total frequency range to the variations in fire intensity for any of the fuel models. The grass types (and hardwood litter) show variations at higher frequencies than do the slash or shrub fuels, and the frequency range tends to increase slightly as the windspeed increases. But in all cases, most of the energy in these spectra is concentrated in a single, narrow frequency-range hump at the low frequency end of the spectrum.

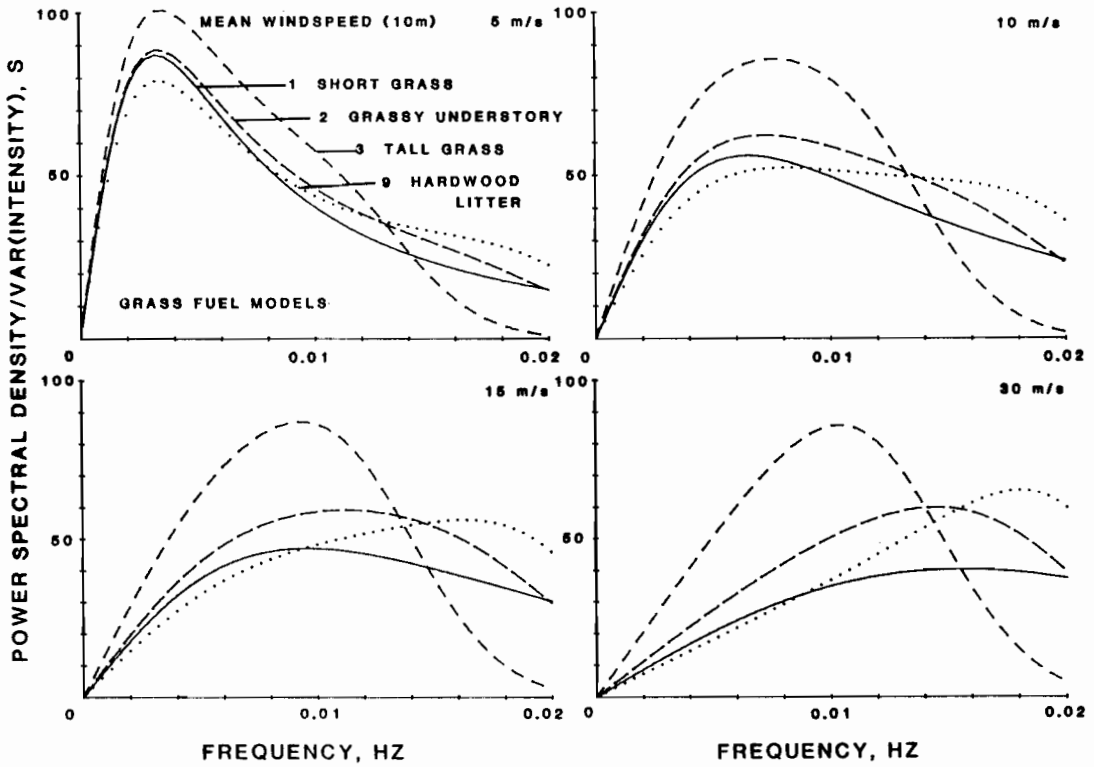

Figure 2.--Power spectral densities of fire intensity variations (divided by variance of intensity) for grass and hardwood litter fuels.

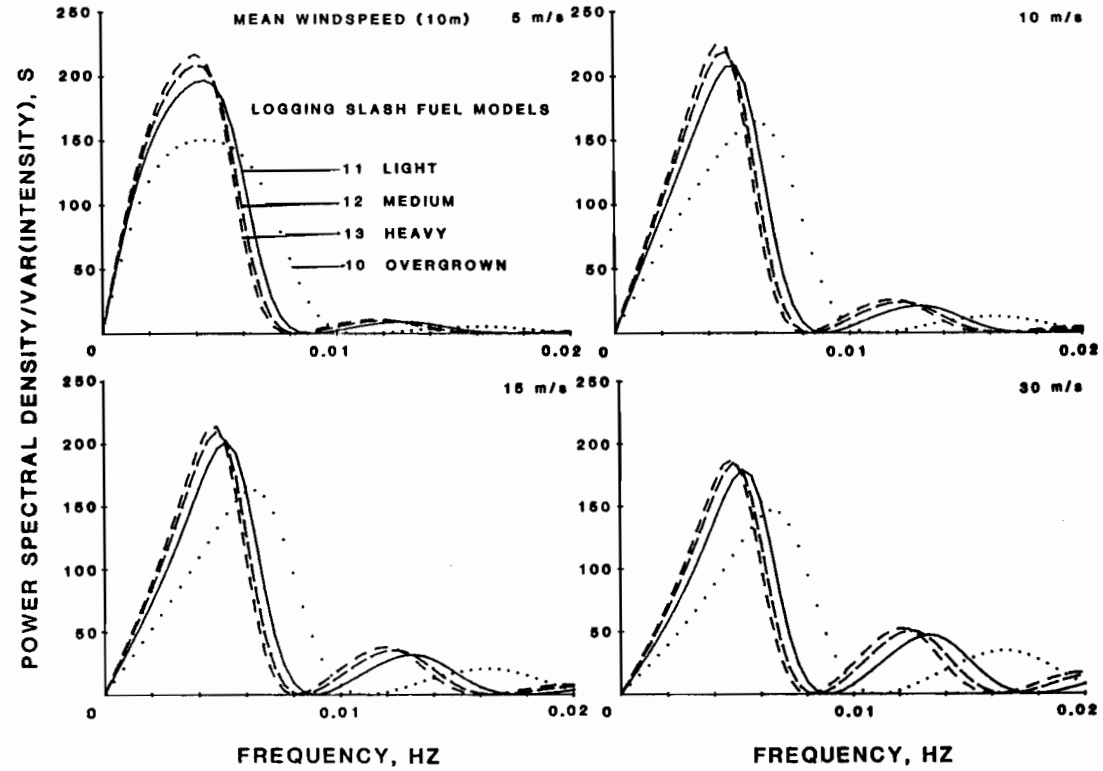

Figure 3.--Power spectral densities of fire intensity variations (divided by variance of intensity) for logging slash fuels.

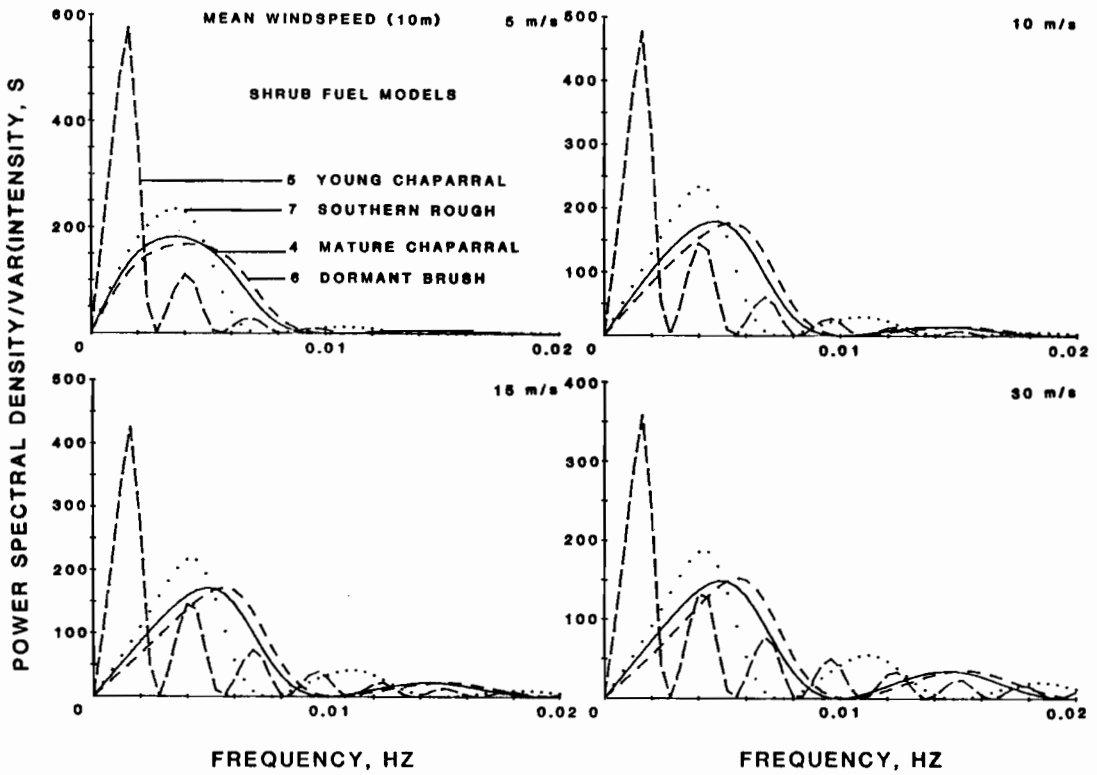

Figure 4.--Power spectral densities of fire intensity variations (divided by variance of intensity) for shrub-type fuels.

Thus much of the information contained in these spectra can be captured in two numbers: (1) the frequency at which the first (lowest frequency) maximum occurs, and (2) the maximum value of the power spectral density. Table 1 lists the frequencies of the first maxima of the power spectra of intensity variations for the twelve fuel models graphed, for windspeeds from 5 to 30 m/s. Table 2 lists the maximum values of the power spectra (normalized by the variance of fire intensity) for the same set of fuel types and windspeeds. These tables can be used as a guide and for numerical data in seeking an approximation to the pattern of fire intensity variations with time.

Such an approximation is necessary because the power spectral density alone does not contain enough information about the variation of intensity with time to reconstruct it (Bendat and Piersol 1966). To predict the strength of a thermal generated by a fluctuation in the intensity level, one needs at least the amplitude of the deviation of intensity from the mean and the duration of the excursion. The extra energy in this excursion could be concentrated in a thermal. The waveform or exact trace of the intensity-vs-time pattern is not important; rather it is the area under such a curve that measures the energy in the deviation. Thus any shape function will suffice, so long as it has the same excess energy in the deviations.

Note that the process for the formation of thermals represents another untestable but very important component of this model. It may be that the thermals shed by a line fire provide the main mechanism of firebrand transport, but that the process by which they are generated is different from that just described. If so, another model for this aspect of the process may be required. Here we assume that it is the low frequency, relatively small amplitude fluctuations of fire intensity that produce the thermals in which we are interested. Another possibility is that relatively rare but more extreme excursions cause them. These kinds of excursions should probably be analyzed as specific events, perhaps using the fire response model (Albini 1982) directly.

The model on which these graphs and tables are based predicts that modest deviations of the intensity from the mean value are most likely to occur as pairs of opposite sign and about equal duration. That is, an increase in intensity will cause the fire spread rate to decrease, leading to a subsequent proportionate decrease in intensity. The duration of the excursions should also be about equal, being fixed by the time it takes the flame front to spread vertically through the fuelbed from top to bottom. It does not matter whether an increase or a decrease occurs first; the same generalization about the behavior obtains.

Table 1. *Frequencies of first maxima of fire intensity power spectra for fuel models without timber cover. Entries are in millihertz.*

Fuel models	Mean horizontal windspeed at 10 m ht, m/s					
	5	10	15	20	25	30
Grass and litter						
1 Short grass	3.2	6.5	9.5	12.1	14.0	15.5
2 Grassy understory	3.4	7.2	11.2	13.0	14.0	14.4
3 Tall grass	3.4	7.6	9.2	9.8	10.2	10.4
9 Hardwood litter	3.4	8.0	16.2	17.2	17.8	18.0
Shrub types						
4 Mature chaparral	3.6	4.6	5.0	5.0	5.0	5.0
5 Young chaparral	1.6	1.6	1.6	1.6	1.6	1.6
6 Dormant brush	4.0	5.4	5.6	5.6	5.6	5.6
7 Southern rough	3.6	4.0	4.2	4.2	4.2	4.2
Logging slash						
10 Overgrown slash	4.4	6.0	6.4	6.4	6.4	6.4
11 Light conifer slash	4.4	5.0	5.2	5.2	5.2	5.2
12 Medium conifer slash	4.0	4.6	4.8	4.8	4.8	4.8
13 Heavy conifer slash	4.0	4.6	4.6	4.8	4.8	4.8

Table 2. *Value of power spectral density/variance at first maximum for fuel models without timber cover. Entries are in seconds.*

Fuel models	Mean horizontal windspeed at 10 m ht, m/s					
	5	10	15	20	25	30
Grass and litter						
1 Short grass	87.0	56.0	47.1	43.5	41.5	40.3
2 Grassy understory	88.7	62.2	59.2	59.7	60.1	59.8
3 Tall grass	100.9	85.6	87.0	87.3	86.8	85.8
9 Hardwood litter	79.2	52.2	56.0	60.8	63.6	65.2
Shrub types						
4 Mature chaparral	182	180	172	162	156	149
5 Young chaparral	576	478	430	393	375	358
6 Dormant brush	168	177	172	165	158	152
7 Southern rough	234	234	219	206	195	187
Logging slash						
10 Overgrown slash	151	165	164	158	152	147
11 Light conifer slash	195	209	202	193	186	179
12 Medium conifer slash	209	220	210	200	192	185
13 Heavy conifer slash	217	226	215	204	195	188

Based on this understanding of the phenomenology, and guided by the fact that only the energy in a deviation of the intensity from the mean for a short time is required to calculate the strength of a thermal, a surrogate process of time-dependent fire intensity is fabricated and analyzed to provide a link between mean fire intensity and the strength of generated thermals. The process invented for analysis consists of a series of deviations from the mean, each being of the same amplitude and each lasting for the same time, but occurring at random intervals of time with a constant long-term average rate. One of these excursions consists of a sudden change in fire intensity from the mean value, followed a short time later by a sudden change of equal magnitude but of the opposite sign, which lasts for the same time. The average value of such an excursion is zero, since it has the same deficit in intensity as it has excess, and the deviations are each of the same duration. Mathematically, one describes such an event as a one-period square wave. The power spectral density of such a sequence of brief oscillations is derived in appendix A.

Figure 5 shows a set of power spectra from the process analyzed. The only parameters needed to describe the sequence are the period--or total duration--of an event, the magnitude of the increase and decrease, and the mean rate of occurrence of the events. The mean rate of occurrence, multiplied by the event period, gives the probability that such an event will be occurring at any arbitrarily selected time of observation. This probability (identified as P_{ON}) is used as a parameter in figure 5, to specify the different curves. The event period is used to multiply the frequency, giving the dimensionless x-axis variable of the graphs. By dividing the power spectral density by the product of the probability parameter, the square of the deviation amplitude, and the event period, the y-axis variable is also made dimensionless.

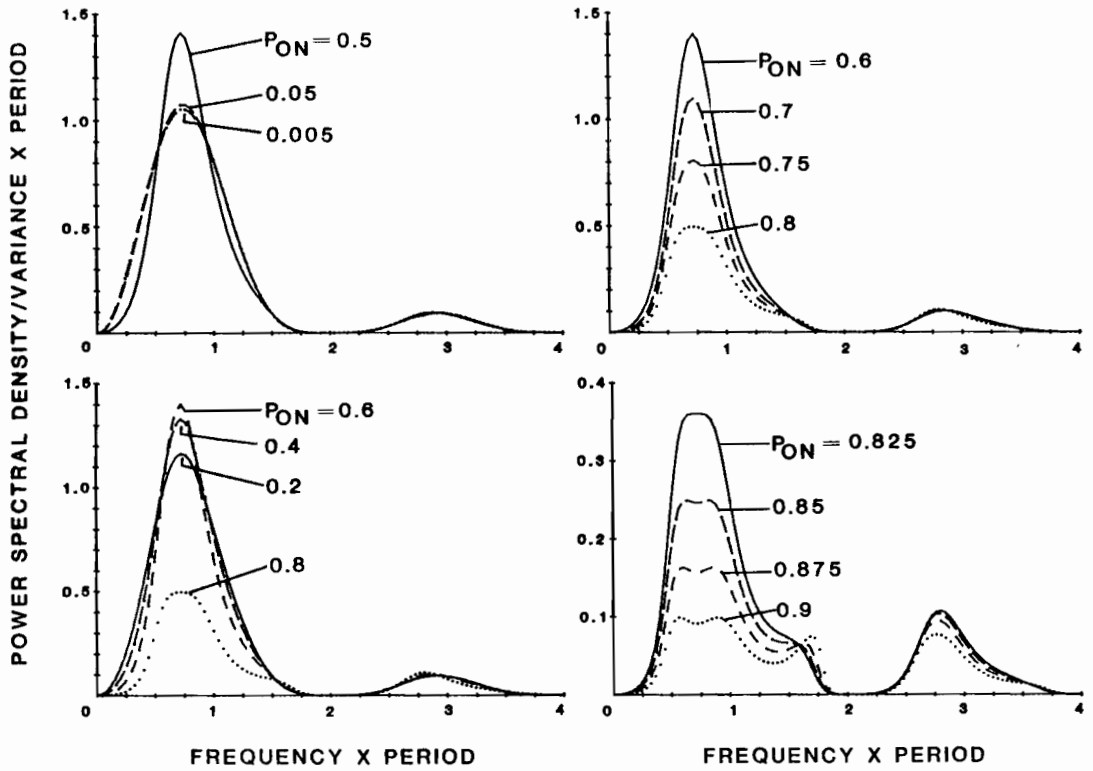

Figure 5.--Power spectral density (divided by product of event period and variance of amplitude) of an ergodic sequence of one-period square wave events with random occurrences. The parameter P_{ON} is the a priori probability that an event is ongoing at any arbitrary point in time. The variance is thus P_{ON} times the mean of the square of the amplitude of the deviations.

The product of the probability and the square of the amplitude is also the variance of the intensity. Thus to match these curves with those given by the modeled fire intensity power spectra in figures 2-4, one need only match the peak of the power spectral density and the frequency at which it occurs. This entails picking a probability value and selecting the event period for the surrogate process. Figure 6 shows examples of the matches that are achieved using this technique.

The graphs in figure 6 illustrate that the match between the hypothetical pattern of intensity variations and that predicted for "real" fires is not very good for the grass and hardwood litter fuels at low windspeed. The surrogate process exaggerates the contribution of the lower frequencies and underestimates the contribution from higher frequencies. The model therefore would tend to overestimate the strengths of the thermals generated, by concentrating too much energy in the intensity deviations assumed. A more realistic waveform would contain more high-frequency components and so reduce the energy in these "square wave thermals". The match to the general shape of the spectra becomes better at higher windspeeds for these fuels. For the slash and shrub fuel types, the match of shapes of the spectra is generally good, at least qualitatively, over the entire range of windspeeds. Again, the errors implied by the nature of the mismatches are such as to overestimate the strengths of the thermals.

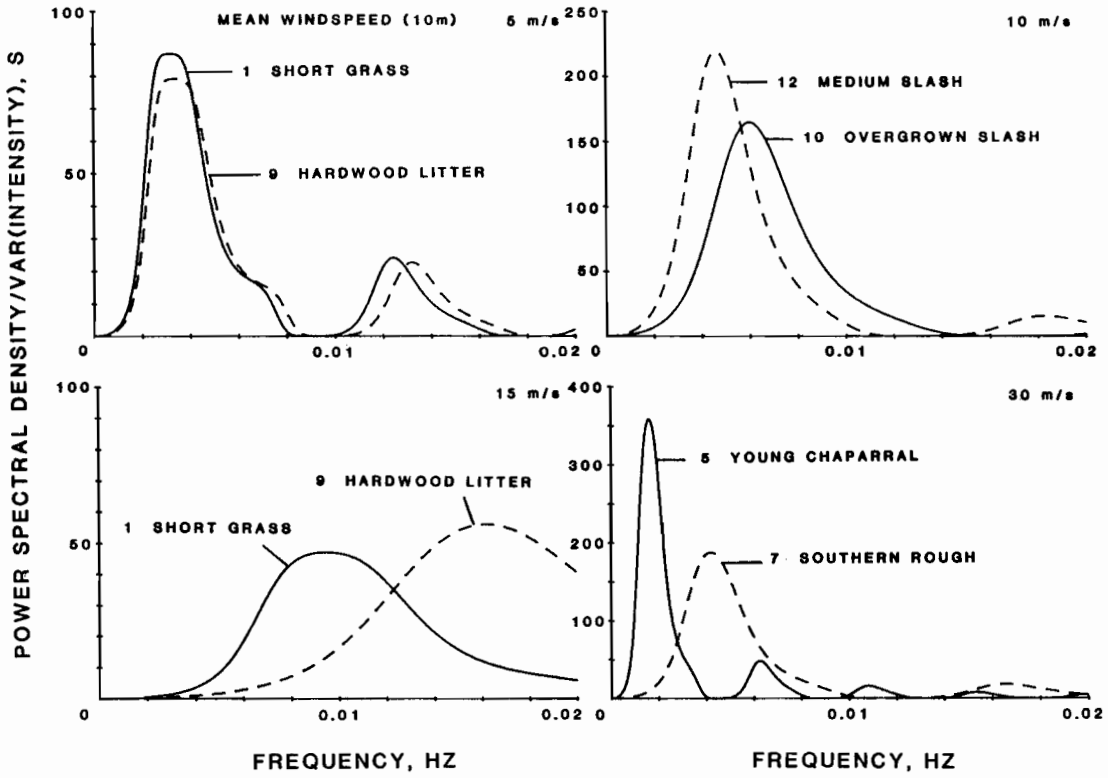

Figure 6.--Results of equating the peak of the power spectral density and the frequency at which it occurs, using the hypothetical spectral density formula derived in appendix A (as graphed in fig. 5) and the predicted power spectral densities for the various fuel models as graphed in figures 2-4. Compare these graphs with the ones they are intended to approximate in figures 2-4.

With the substitution of the hypothetical process for the actual but unknown fire intensity variation pattern, the energy in a thermal becomes very easy to calculate. It is simply the product of the magnitude of the intensity variation multiplied by half the event period. The period is determined by matching the frequencies of the peaks of the power spectra, and the magnitude of the deviations is determined by matching the peak values of the power spectra. The resulting expression for the energy in a thermal becomes a numerical constant multiplied by the standard deviation of the fire intensity variations and divided by the frequency of the peak in the power spectrum. This form could have been predicted at the outset purely from dimensional arguments. The numerical values of the constants are the only quantities that depend upon the specific model chosen as a surrogate for the real variations in fire intensity. For that reason, the details of this substituted process are of no great consequence to the predictions of this model.

The value of the standard deviation of fire intensity, expressed as a percentage of the mean fire intensity, is presented for the 12 fuel models analyzed in table 3. These results are predicted directly by the intensity fluctuation model (Albini 1983a) and do not depend at all on the substitute process. Note that the fractions in table 3 decline with increasing windspeed. This does not mean that the strength of the thermals decreases with windspeed. On the contrary, because the mean fire intensity increases with windspeed faster than the percentage deviations decrease, and the periodicity remains about constant, the thermals in fact become stronger.

Table 3. *Values of the standard deviation of fire intensity, as a percentage of the mean intensity (coefficient of variation) for 12 fuel models that occur without timber cover.*

Fuel model	Mean horizontal windspeed at 10 m ht, m/s					
	5	10	15	20	25	30
Grass and litter						
1 Short grass	12.5	9.30	7.36	6.01	5.03	4.28
2 Grassy understory	18.8	15.2	12.5	10.4	8.79	7.54
3 Tall grass	16.4	12.0	9.09	7.12	5.74	4.75
9 Hardwood litter	23.5	21.2	18.9	16.7	14.9	13.3
Shrub types						
4 Mature chaparral	13.3	8.27	5.76	4.34	3.43	2.82
5 Young chaparral	8.11	4.70	3.33	2.59	2.11	1.79
6 Dormant brush	16.2	11.0	8.06	6.28	5.10	4.28
7 Southern rough	14.4	9.19	6.63	5.14	4.18	3.51
Logging slash						
10 Overgrown slash	18.3	13.3	10.2	8.19	6.84	5.87
11 Light conifer slash	17.1	11.8	8.87	7.07	5.86	5.01
12 Medium conifer slash	16.3	11.0	8.13	6.43	5.30	4.50
13 Heavy conifer slash	16.0	10.7	7.92	6.26	5.16	4.38

The final step in this lengthy process is to relate the strengths of the thermals to the mean fire intensity and windspeed for each fuel model:

$$E = I\ f(U) \tag{7}$$

where E is the strength of a thermal (kJ/m), I is mean fire intensity (kW/m), and f(U) is a function of the mean windspeed at 10 m height. This function was found by fitting a power law of the form:

$$f(U) = A\ U^{B} \tag{8}$$

(f in units of seconds) to the numerical results obtained for each of the 6 windspeeds used in the tables above. By this process, the simple final results given in table 4 were derived.

Table 4. *Results of power law regressions to approximate the energy in line thermals generated by burning various fuels. E/I = A exp (B log U) where E is the energy in a thermal and I is mean fire intensity. Units of coefficient A are in seconds and U is 10-m height mean windspeed, m/s.*

Fuel model	A (s)	B	Coefficient of determination
Grass and litter			
1 Short grass	162	-1.456	1.000
2 Grassy understory	166	-1.282	.998
3 Tall grass	129	-1.238	.996
9 Hardwood litter	154	-1.151	.979
Shrub types			
4 Mature chaparral	83.9	-1.040	1.000
5 Young chaparral	94.4	- .881	1.000
6 Dormant brush	74.1	- .906	1.000
7 Southern rough	75.1	- .884	.998
Logging slash			
10 Overgrown slash	66.1	- .810	.998
11 Light conifer slash	63.6	- .776	.993
12 Medium conifer slash	69.6	- .818	.997
13 Heavy conifer slash	71.8	- .835	.995

SPOTTING DISTANCE EXAMPLES

To illustrate the use of the formulation presented here, two examples are computed. In the first example, we estimate the maximum spotting distance from a wind-driven fire in short grass; in the second example the fuel is chaparral, and we consider a higher windspeed. For simplicity, the terrain is considered to be flat in both cases.

Example 1. Estimate the maximum spot fire distance from a heading fire in short grass, with intensity of 2000 kW/m (580 Btu/ft-s) when the mean windspeed at 10-m height is 5 m/s (about 11 mi/h).

We must use equation (7) to find the energy (E) in a thermal from the line fire. We have the intensity (I), so we refer to table 4 to find the parameters defining the multiplying function f(U). Table 4 gives, for short grass, A = 162, B = -1.465. The windspeed (U) is 5 m/s, so the multiplying function f(U) is given by

$$f(U) = A\ U^{B} = 162 \times (5)^{-1.465} = 15.33\ \text{s}. \qquad (9)$$

Multiplying this factor by the intensity (I = 2000 kW/m) gives the thermal energy:

$$E = I\ f(U) = (2000) \times (15.33) = 30\ 660\ \text{kJ/m}. \qquad (10)$$

This energy is used in equation (2) to obtain the maximum firebrand particle height, H:

$$H = 0.173\ E^{1/2} = 0.173 \times (30\ 660)^{1/2} = 30\ \text{m}. \qquad (11)$$

This quantity is the initial firebrand particle height. Using the formulae in Chase (1981), where this height is called z(0), we find that the cover height associated with short grass is too low to allow use of the logarithmic windspeed profile, and that we must use instead an "effective cover height" (Albini 1981a) of 1.93 m to calculate the maximum spotting distance. Using the formula in Chase (1981), p. 5, for the flat-terrain spotting distance, there labeled F, we discover that we require the windspeed (in km/h) at 6 m height. We can obtain this from equation (4), using the power law profile for windspeed with height. We use this profile because it is convenient and closely approximates the logarithmic law, although either could be used without introducing error beyond that probably inherent in the model.

Using equation (4), we estimate the windspeed at 6 m height to be:

$$U(6\text{m}) = U(10\text{m}) \times (6/10)^{1/7} = 0.93 \times U(10\text{m})$$

$$= 0.93 \times 5 = 4.65\ \text{m/s} = 16.7\ \text{km/h}. \qquad (12)$$

This windspeed can be used in the equation in Chase (1981) to calculate the maximum spotting distance, with the result:

$$F = \text{flat terrain spotting distance} = 0.17\ \text{km}. \qquad (13)$$

To this distance it is necessary to add the downwind drift during lofting, from equation (3). That equation requires the windspeed at the maximum particle height. Again we return to equation (4) to estimate that value, with the result:

$$U(30m) = U(10m) \times (30/10)^{1/7} = 5 \times 1.17 = 5.85 \text{ m/s}. \quad (14)$$

Using this value in equation (3) gives the spotting distance correction as:

$$X = 2.78 \times 5.85 \times (30)^{1/2} = 89 \text{ m} = 0.09 \text{ km}. \quad (15)$$

This result illustrates the importance of the correction term in this instance, since this distance is about half that predicted due to falling from the initial height in the wind. Adding the correction to the original prediction (12), gives the final result of 0.26 km (or about 0.16 mi).

Example 2. Estimate the maximum spot fire distance from a wind-driven fire in chaparral, when the windspeed at 10 m height is 20 m/s and the fire intensity is calculated to be 50 000 kW/m (about 14,400 Btu/ft-s).

This is a severe surface fire with very high intensity and very strong wind. Large spotting distances might be expected, especially in light of the results of the first example.

Again, the first step is to estimate the strength of the thermals from the line fire. Table 4 gives the values A = 83.9 and B = -1.04. Using these in the equation for f(U)--equation (8)--gives a multiplier of

$$f(U) = A\ U^{B} = (83.9) \times (20)^{-1.04} = 3.72 \text{ s}, \quad (16)$$

and so a thermal strength, from equation (7), of

$$E = I\ f(U) = (50\ 000) \times (3.72) = 186\ 000 \text{ kJ/m}. \quad (17)$$

Using this result in equation (2) gives the maximum firebrand lofting height

$$H = 0.173\ E^{1/2} = 0.173 \times (431) = 75 \text{ m}. \quad (18)$$

As before, it is necessary to estimate the windspeed at 6 m height, and again we can use equation (4). Doing so gives the value 66.9 km/h at the lower height. Also as in the previous case, the formulation in Chase (1981) restricts us to use of the power law windspeed profile, and hence to use of an artificial cover height. With these data in hand, Chase's formula gives a flat-terrain spotting distance (F) of 1.26 km.

The downwind drift during particle lofting again is a large correction to this result. Once more using equation (4) to extrapolate the windspeed to the firebrand height, we find

$$U(75m) = U(10\ m) \times (75/10)^{1/7} = 26.7 \text{ m/s}. \quad (19)$$

This result, used in equation (3), gives the correction to be added to the predicted spotting distance:

$$X = 2.78 \times (26.7) \times (75)^{1/2} = 642 \text{ m} = 0.64 \text{ km}. \qquad (20)$$

The final result in this case is 1.26 + 0.64 = 1.90 km, or about 1.2 mi. This result may seem to be a low estimate. Note, however, that even with this high intensity, equation (1) predicts that the wind field should overpower the convection column and blow the smoke along the surface. In such situations, long range spotting is infrequent.

SUMMARY

The process by which firebrands are transported from wind-driven line fires is postulated to be that of lofting of particles by line thermals that are generated by variations in the intensity of the fire. Both the mechanism of firebrand lofting and the mechanism of the generation of thermals are speculative assumptions that are probably not directly subject to test. Because of this fact, the model presented here is a theoretical construct and will probably remain so, even if field tests show its predictions to be usefully accurate. The motivation for this approach is simply that the problem in its general form is analytically intractable, being both three-dimensional and time-dependent. This analysis preserves the appealing idealization of two-dimensionality, but incorporates in a weak way the time variability. The postulation of a surrogate time sequence process representing the fire intensity variations permits direct computation of the strength of thermals generated by a line fire, with little additional distortion suspected. Equations presented here permit direct computation of the maximum firebrand lofting height and the drift downwind during lofting, given the mean intensity of the fire, the mean windspeed at 10 m height, and a fuel description in terms of one of twelve stylized models widely used for predicting the behavior of wildland fires. From the maximum firebrand lofting height, the maximum spotting distance is calculable using equations and graphs available in earlier publications or published pocket calculator algorithms.

PUBLICATIONS CITED

Albini, Frank A. Estimating wildfire behavior and effects. Gen. Tech. Rep. INT-30. Ogden, UT: U.S. Department of Agriculture, Forest Service, Intermountain Forest and Range Experiment Station; 1976. 92 p.

Albini, Frank A. Spot fire distance from burning trees--a predictive model. Gen. Tech. Rep. INT-56. Ogden, UT: U.S. Department of Agriculture, Forest Service, Intermountain Forest and Range Experiment Station; 1979. 73 p.

Albini, Frank A. Spot fire distance from isolated sources--extensions of a predictive model. Res. Note INT-309. Ogden, UT: U.S. Department of Agriculture, Forest Service, Intermountain Forest and Range Experiment Station; 1981a. 9 p.

Albini, Frank A. A model for the wind-blown flame from a line fire. Comb. Flame 43:155-174. 1981b.

Albini, Frank A. Response of free-burning fires to nonsteady wind. Comb. Sci. Technol. 29:225-241; 1982.

Albini, Frank A. The variability of wind-aided free-burning fires. Comb. Sci. Technol. (in press); 1983a.

Albini, Frank A. Transport of firebrands by line thermals. Comb. Sci. Technol. (in press); 1983b.

Bendat, Julius S.; Piersol, Allan G. Measurement and analysis of random data. New York: John Wiley & Sons; 1966. 390 p.

Brown, A. A.; Davis, K. P. Forest fire: control and use. New York: McGraw-Hill; 1973. 686 p.

Byram, G. M. Combustion of forest fuels. In Davis, Kenneth P., ed., Forest fire control and use. New York: McGraw-Hill Book Co.; 1959; 584 p.

Cederwall, Klas. Buoyant slot jets into stagnant or flowing environments. Rep. No. KH-R-25. Pasadena, CA: W. M. Keck Laboratory of Hydraulics and Water Resources, Div. Engrg. Appl. Sci., Calif. Inst. Tech.; 1971. 86 p.

Chase, Carolyn H. Spot fire distance equations for pocket calculators. Res. Note INT-310. Ogden, UT: U.S. Department of Agriculture, Forest Service, Intermountain Forest and Range Experiment Station; 1981. 19 p.

Davenport, A. G. The spectrum of horizontal gustiness near the ground in high winds. J. Roy. Meteorol. Soc. 87(372):194-211; 1961.

Doran, J. C.; Powell, D. C. Gust structure in the neutral boundary layer. J. Appl. Meteorol. 21(1):14-17; 1982.

Fernandez-Pello, A. C.; Mao, C. P. A unified analysis of concurrent modes of flame spread. Comb. Sci. Technol. 26:147-155; 1981.

Gostintsev, Yu. A.; Sukhanov, L. A. Convective column above a linear fire in a homogeneous isothermal atmosphere. Fizika Goreniya i Vzryva 13(5):675-685; 1977.

Gostintsev, Yu. A.; Sukhanov, L. A. Convective column above a linear fire in a polytropic atmosphere. Fizika Goreniya i Vzryva 14(3):3-8; 1978.

Lee, Shao-Lin; Emmons, H. W. A study of natural convection above a line fire. J. Fld. Mech. 11(3):353-368; 1961.

Luke, R. H.; McArthur, A. G. Bushfires in Australia. Canberra, ACT: Australian Govt. Publ. Serv.; 1978. 359 p.

Luti, F. Makau. Transient flow development due to a strong heat source in the atmosphere Part I: Uniform temperature source. Comb. Sci. Technol. 23:163-175; 1980.

Luti, F. Makau. Some characteristics of a two-dimensional starting mass fire with cross flow. Comb. Sci. Technol. 26:25-33; 1981.

Monteith, J. L. Principles of environmental physics. New York: American Elsevier Publ. Co.; 1973. 241 p.

Plate, Erich J. Aerodynamic characteristics of atmospheric boundary layers. U.S. Atomic Energy Commission (now Dept. Energy) [NTIS TID-25465]; 1971. 190 p.

Priestley, C. H. B.; Ball, F. K. Continuous convection from an isolated source of heat. Quart. J. Roy. Meteorol. Soc. 81:144-157; 1955.

Putnam, A. A. A model study of wind-blown free-burning fires. Tenth Symp. (Intl.) Comb. Proc. 1964:1039-1046. Pittsburgh, PA: Comb. Inst.; 1965.

Rankine, A. O. Experimental studies in thermal convection. Proc. Phys. Soc. (A) 63(5):417-443; 1950.

Richards, J. M. Experiments on the motions of isolated cylindrical thermals through unstratified surroundings. Intl. J. Air Wat. Poll. 7:17-34; 1963.

Roberts, Philip J. W. Dispersion of buoyant waste water discharged from outfall diffusers of finite length. Rep. No. KH-R-35. Pasadena, CA: W. M. Keck Laboratory of Hydraulics and Water Resources, Div. Engrg. Appl. Sci., Calif. Inst. Tech.; 1977. 214 p.

Roberts, Philip J. W. Line plume and ocean outfall dispersion. J. Hydraulics Div. ASCE 105(HY4):313-331; 1979a.

Roberts, Philip J. W. Two-dimensional flow field of multiport diffuser. J. Hydraulics Div., ASCE 105(HY5):607-611; 1979b.

Roberts, Philip J. W. Ocean outfall dilution: effects of currents. J. Hydraulics Div., ASCE 106(HY5):769-782; 1980.

Rothermel, Richard C. How to predict the spread and intensity of forest and range fires. Ogden, Utah: U.S. Department of Agriculture, Forest Service, Intermountain Forest and Range Experiment Station; (in process); 1983.

Rouse, Hunter. Gravitational diffusion from a boundary source in two-dimensional flow. J. Appl. Mech. A225-A228; 1947.

Rouse, Hunter; Yih, C. S.; Humphreys, H. W. Gravitational convection from a boundary source. Tellus 4:201-210; 1952.

Saaty, T. L. Mathematical methods of operations research. McGraw-Hill, New York. 1959. 421 pp.

Scorer, R. S. The behavior of chimney plumes. Intl. J. Air Poll. 1:198-220; 1959.

Strobel, F. A.; Chen, T. S. Buoyancy effects on heat and mass transfer in boundary layers adjacent to inclined, continuous, moving sheets. Numerical Heat Transfer 3:461-481; 1980.

Taylor, G. I. Fire under influence of natural convection. 10-31 in Berl, W. G., ed., The use of models in fire research. Natl. Acad. Sci. Publ. 786. Washington, D.C.: Natl. Acad. Sci. - Natl. Resch. Found.; 1961. 321 p.

Van Wagner, C. E. Height of crown scorch in forest fires. Can. J. For. Res. 3(3):373-378; 1973.

APPENDIX A: POWER SPECTRAL DENSITY OF AN ERGODIC SEQUENCE OF ONE-PERIOD 'SQUARE WAVE' EVENTS

Process Description

A process described by a function of time that is in some sense unpredictable is said to be stochastic. Here we consider the stochastic process described by the function x(t), where t is time,

$$x(t) = x_o + \sum_{i=-\infty}^{+\infty} W(t - t_i) \tag{1}$$

x_o is the mean or long-term average of x, the times t_i are random, and W is a "square wave" of amplitude A and period T:

$$W(t') = \begin{cases} 0 & t' \leq 0 \\ A & 0 < t' < T/2 \\ 0 & t' = T/2 \\ -A & T/2 < t' < T \\ 0 & t' \geq T. \end{cases} \tag{2}$$

It is further stipulated that the times t_i are sufficiently separated that the waveforms of the various one period deviations of x(t) from x_o do not overlap:

$$|t_i - t_j| \geq T;\ i \neq j. \tag{3}$$

The realization of x(t) expressed by (1)-(3) can be visualized as a sequence of events which occur at random times. An "event" is the deviation of x(t) from its mean value, x_o. As time goes on, these events recur; but while an event is ongoing ($t_i < t < t_i + T$), another event cannot occur. For simplicity, we assume here that the amplitude, A, and duration, T, of each event is the same. These restrictions can be relaxed later if necessary.

A more powerful constraint that we shall not relax is the assumption that the process is ergodic. For the process under discussion, this can be stated as a requirement that the time elapsed between sequential events can be described as a random variable, whose distribution function is independent of time. This simple requirement ensures that the statistical properties of any finite sample of the function x(t) do not depend *a priori* upon when the sample is taken. Therefore an ensemble of such finite samples can be substituted, conceptually, for a single time stream sample of the same total duration. The equivalence of ensemble-averaged and time-averaged statistics is of enormous analytical consequence.

Specifically, let f(θ) be the probability density function for the distribution of times (θ) that elapse between the end of one event and the beginning of the next. If f(θ) does not depend upon t, then the process described will be ergodic. For example, with a large enough sample, the average time lapse between events, T_L, will approach the mean of the distribution f(θ):

$$T_L \to \int_0^\infty \theta f(\theta) d\theta. \tag{4}$$

Autocorrelation Function

A characterization of the process x(t) in terms of its frequency content is expressed by its power spectral density, $S_x(n)$, where n is frequency. The most direct approach to derivation of S_x is through use of the autocorrelation function of the process, $C_x(\tau)$:

$$C_x(\tau) = \lim_{t\to\infty} \frac{1}{t}\int_{-t/2}^{+t/2} x(t')x(t' + \tau)dt'. \quad (5)$$

Because we are dealing with a mathematically real process, C_x is an even function of τ and the power spectrum can be written as the cosine transform of C_x (Bendat and Piersol, 1966):

$$S_x(n) = 4\int_0^\infty \cos(2\pi n\tau)C_x(\tau)d\tau. \quad (6)$$

Without loss of generality, the mean, x_o, can be taken to be zero. Then $C_x(0)$ becomes the variance of the process and a singularity at n = 0 is removed from $S_x(n)$.

Making use of the ergodic property of the process, the time averaging operation of (5) can be replaced by an ensemble average, expressed here as the expectation operator E:

$$C_x(\tau) = E(x(t)x(t + \tau)). \quad (7)$$

The expected value of the product $x(t)x(t + \tau)$ can be deduced (conceptually) by sampling the value of the product uniformly over a large ensemble of records of the function x(t). The product clearly can take on only three values, namely A^2, $-A^2$, and 0. The task at hand is to describe, as a function of τ, the fraction of the samples that would have each of these values, given the distribution function for the time lapse between events, $f(\theta)$.

Consider first the value of x(t). It will be nonzero only a fraction of the time (or for only a fraction of the number of samples, for any given time on the record of each sample). This fraction can be interpreted as P_{ON}, the *a priori* probability that an event will be ongoing at any arbitrarily selected time during a sample record. If we consider a long-duration record with a total time span T*, then the number of events that we should expect to observe during that time is N*, where the total time during which events are occurring can be expressed as

$$N^*T = P_{ON}T^*. \quad (8)$$

But the average time elapsed between events is T_L (Eq. 4), so the total timespan should also be expressable as

$$T^* = N^*(T_L + T). \quad (9)$$

Hence the probability that an event is ongoing at any arbitrary time is

$$P_{ON} = T/(T_L + T), \quad (10)$$

and the mean rate of occurrence of events, ν, is

$$\nu = N^*/T^* = 1/(T_L + T) = P_{ON}/T. \quad (11)$$

We can now express (7) in terms of a conditional expectation $\gamma(\tau)$, where

$$\gamma(\tau) = E(x(t)x(t + \tau) \,|\, x(t) \neq 0), \tag{12}$$

by which we mean the expected value of $x(t)x(t + \tau)$, given that $x(t)$ is not zero. Depending upon τ, the product can still vanish because the second factor may be zero, but in general

$$C_x(\tau) = P_{ON}\gamma(\tau). \tag{13}$$

Because $\gamma(0)$ is A^2, we can normalize (13) by the variance of the process and deal with the normalized conditional autocorrelation function, G:

$$C_x(\tau)/\sigma^2 = C_x(\tau)/P_{ON}A^2 = \gamma(\tau)/A^2 = G(\tau). \tag{14}$$

To express $G(\tau)$ explicitly, it is necessary to introduce the additional conditional probability function, $P(\theta)$. This function represents the distribution of probability that an event starts at time θ after the cessation of a given event, whether or not one or more intervening events. Specifically,

$$\Pr\left\{\begin{matrix}\text{an event starts at time } (\theta,\theta+d\theta) \\ \text{after a given event ceases}\end{matrix}\right\} = P(\theta)d\theta. \tag{15}$$

This function can be defined by the recursion:

$$P(\theta) = \begin{cases} f(\theta), & \theta < T \\ f(\theta) + \displaystyle\int_0^{\theta-T} f(x)P(\theta - T - x)dx, & \theta \geq T\ . \end{cases} \tag{16}$$

Recall that $f(\theta)$ represents the probability distribution function for the beginning of the next event after the one whose cessation marks the origin of relative time, θ. The integral in (16) can be evaluated for $2T > \theta \geq T$ by using f for P in accordance with (16), and extended by recursively applying the same algorithm. Note that no closure condition applies to the conditional distribution P. It does apply to f, however, which means that the asymptotic solution to (16) is a constant. P must become independent of the time origin for large θ and indeed should approach the mean rate of occurrence, ν (Eq. 11):

$$\lim_{\theta \to \infty} P(\theta) = \nu. \tag{17}$$

The function P will obviously be complicated if written explicitly, but its use symbolically allows compact notation for the correlation function G.

To express G explicitly, we can imagine examining the statistics of the product $x(t)x(t+\tau)$ formed from a large sample of such, all satisfying the stipulation that $x(t) \neq 0$. This is equivalent to placing a relative time origin somewhere within the period of one event with uniform probability, noting the value of x at that point, and forming its product with the expected value of x at a time τ later. This conceptual artifice allows us to write the following expressions by inspection:

$$0 \le \tau \le T/2: \quad G(\tau) = \int_0^{T/2-\tau} \frac{dt}{T} - \int_{T/2-\tau}^{T/2} \frac{dt}{T} + \int_{T/2}^{T-\tau} \frac{dt}{T} - \int_{T-\tau}^{T} \int_0^{t+\tau-T} P(\theta)d\theta \, \frac{dt}{T} \tag{18}$$

$$T/2 \le \tau \le T: \quad G(\tau) = -\int_0^{T-\tau} \frac{dt}{T} + \int_{T-\tau}^{T/2} \int_0^{t+\tau-T} P(\theta)d\theta \, \frac{dt}{T} - \int_{T/2}^{T} \int_{\max(0,t+\tau-3T/2)}^{t+\tau-T} P(\theta)d\theta \, \frac{dt}{T}$$

$$+ \int_{3T/2-\tau}^{T} \int_0^{t+\tau-3T/2} P(\theta)d\theta \, \frac{dt}{T} \tag{19}$$

$$T \le \tau \le 3T/2: \quad G(\tau) = \int_0^{T/2} \int_{\max(0,t+\tau-3T/2)}^{t+\tau-T} P(\theta)d\theta \, \frac{dt}{T} + \int_{T/2}^{T} \int_{\max(0,t+\tau-2T)}^{t+\tau-3T/2} P(\theta)d\theta \, \frac{dt}{T}$$

$$- \int_{3T/2-\tau}^{T/2} \int_0^{t+\tau-3T/2} P(\theta)d\theta \, \frac{dt}{T} - \int_{T/2}^{T} \int_{t+\tau-3T/2}^{t+\tau-T} P(\theta)d\theta \, \frac{dt}{T} \tag{20}$$

$$3T/2 \le \tau \le 2T: \quad G(\tau) = \int_0^{T/2} \int_{t+\tau-3T/2}^{t+\tau-T} P(\theta)d\theta \, \frac{dt}{T} + \int_{T/2}^{T} \int_{t+\tau-2T}^{t+\tau-3T/2} P(\theta)d\theta \, \frac{dt}{T}$$

$$- \int_0^{T/2} \int_{\max(0,t+\tau-2T)}^{t+\tau-3T/2} P(\theta)d\theta \, \frac{dt}{T} - \int_{T/2}^{T} \int_{t+\tau-3T/2}^{t+\tau-T} P(\theta)d\theta \, \frac{dt}{T} \tag{21}$$

$$2T \le \tau: \quad G(\tau) = \int_0^{T/2} \int_{t+\tau-3T/2}^{t+\tau-T} P(\theta)d\theta \, \frac{dt}{T} + \int_{T/2}^{T} \int_{t+\tau-2T}^{t+\tau-3T/2} P(\theta)d\theta \, \frac{dt}{T}$$

$$- \int_0^{T/2} \int_{t+\tau-2T}^{t+\tau-3T/2} P(\theta)d\theta \, \frac{dt}{T} - \int_{T/2}^{T} \int_{t+\tau-3T/2}^{t+\tau-T} P(\theta)d\theta \, \frac{dt}{T} . \tag{22}$$

These expressions can be simplified somewhat, but first note that by integrating (6) twice by parts and using (14), we have, for a suitably continuous and differentiable $G(\tau)$:

$$\frac{(\pi n)^2 S_x(n)}{P_{ON} A^2} = -G'(0) - \int_0^{\infty} \cos(2\pi n\tau) G''(\tau) d\tau \tag{23}$$

where the number of prime signs indicates the number of differentiations with respect to the argument.

Power Spectral Density

Integration by parts and simplification before differentiating helps in deriving the second derivative form needed for evaluating (23). Note from (22), however, that $G(\tau)$ vanishes for large τ if P becomes constant, and $G''(\tau)$ must also vanish. Performing the indicated operations gives the piecewise continuous functionals G' and G":

$0 \le \tau \le T/2$:
$$G'(\tau) = -3/T - \int_0^{\tau} P(\theta)d\theta/T \tag{24}$$

$T/2 \le \tau \le T$:
$$G'(\tau) = 1/T + (3/T)\int_0^{\tau-T/2} P(\theta)d\theta - \int_{\tau-T/2}^{\tau} P(\theta)d\theta/T \tag{25}$$

$T \le \tau \le 3T/2$:
$$G'(\tau) = (3/T)\left\{\int_{\tau-T}^{\tau-T/2} P(\theta)d\theta - \int_0^{\tau-T} P(\theta)d\theta\right\} - \int_{\tau-T/2}^{\tau} P(\theta)d\theta/T \tag{26}$$

$3T/2 \le \tau \le 2T$:
$$G'(\tau) = (3/T)\left\{\int_{\tau-T}^{\tau-T/2} P(\theta)d\theta - \int_{\tau-3T/2}^{\tau-T} P(\theta)d\theta\right\} + (1/T)\left\{\int_0^{\tau-3T/2} P(\theta)d\theta - \int_{\tau-T/2}^{\tau} P(\theta)d\theta\right\} \tag{27}$$

$2T \le \tau$:
$$G'(\tau) = (1/T)\left\{\int_{t-T/2}^{t-3T/2} P(\theta)d\theta - \int_{\tau-T/2}^{\tau} P(\theta)d\theta\right\} + (3/T)\left\{\int_{\tau-T}^{\tau-T/2} P(\theta)d\theta - \int_{\tau-3T/2}^{\tau-T} P(\theta)d\theta\right\} \tag{28}$$

$0 \le \tau \le T/2$:
$$G''(\tau) = -P(\tau)/T \tag{29}$$

$T/2 \le \tau \le T$:
$$G''(\tau) = -P(\tau)/T + (4/T)P(\tau - T/2) \tag{30}$$

$T \le \tau \le 3T/2$:
$$G''(\tau) = -P(\tau)/T + (4/T)P(\tau - T/2) - (6/T)P(\tau - T) \tag{31}$$

$3T/2 \le \tau \le 2T$:
$$G''(\tau) = -P(\tau)/T + (4/T)P(\tau - T/2) - (6/T)P(\tau - T) + (4/T)P(\tau - 3T/2) \tag{32}$$

$2T \le \tau$:
$$G''(\tau) = -P(\tau)/T + (4/T)P(\tau - T/2) - (6/T)P(\tau - T) + (4/T)P(\tau - 3T/2) - (1/T)P(\tau - 2T). \tag{33}$$

Now because $G'(\tau)$ is discontinuous, the simple form of (23) cannot be used directly. It is necessary instead to evaluate the contributions of each of the discontinuous segments due to the differences in the value of G' as approached from opposite directions at each matching point.

The appearance of the functions of shifted arguments in each of the above expressions coincides with the breaks in applicability of the expressions, leading to a particularly simple form (using circular frequency ω for $2\pi n$) for the contribution of G" to the power spectrum:

$$-\int_0^{\infty} \cos(\omega\tau)G''(\tau)d\tau = \int_0^{\infty} P(\tau)\Gamma(\tau)d\tau/T. \tag{34}$$

Here

$$\Gamma(\tau) = \cos(\omega\tau)-4\cos(\omega\tau+\omega T/2)+6\cos(\omega\tau+\omega T)-4\cos(\omega\tau+3\omega T/2)+\cos(\omega\tau+2\omega T), \qquad (35)$$

which can be shown to be

$$\Gamma(\tau) = 16\sin^4(\omega T/4)\cos(\omega\tau + \omega T). \qquad (36)$$

The contributions to (23) of the discontinuities of $G'(\tau)$ consist of a sum of terms of the form

$$\cos(k\omega T/2)[G'_+(kT/2) - G'_-(kT/2)] \qquad (37)$$

where k = 1,2,3, or 4 and the subscript sign implies the direction of approach to the discontinuity. Thus to (23) we must add the following sum, due to the differences between the limits of (24) and (25) and (25) and (26):

$$-(4/T)\cos(\omega T/2) + (1/T)\cos(\omega T).$$

Thus we have the relatively simple form for the power spectrum:

$$\begin{aligned}\frac{\omega^2 T\, S_x(n)}{4P_{ON}A^2} &= 3 - 4\cos(\omega T/2) + \cos(\omega T) \\ &\quad + 16\sin^4\left(\frac{\omega T}{4}\right)\int_0^\infty \cos(\omega\tau+\omega T)P(\tau)d\tau \\ &= 8\sin^4\left(\frac{\omega T}{4}\right)\left\{1 + 2\int_0^\infty P(\tau)\cos(\omega\tau+\omega T)d\tau\right\}. \qquad (38)\end{aligned}$$

Uniform Occurrence Rate Probabilities

The simple form of (38) rests upon the hidden complexity of the ubiquitous conditional probability function $P(\theta)$. This function is determined by the probability density function for the occurrence of the next subsequent event, $f(\theta)$, as expressed in (16). To express $f(\theta)$ and $P(\theta)$ analytically, we invoke this assumption:

> Given the condition that an event is not ongoing, the probability that an event begins in the next differential element of time, dt, is μdt, where μ is constant.

This assumption is very widely used in the mathematical analysis of queueing processes (Saaty 1959) and, in the limit of zero event duration, leads to a Poisson distribution for the number of events in a finite time.

Using this assumption, one readily can show that the probability density $f(\theta)$ for the occurrence of the next subsequent event is

$$f(\theta) = \mu\exp(-\mu\theta). \qquad (39)$$

The mean time lapse between events (eq. 4) is thus $1/\mu$, and the longterm probability that an event is ongoing at any arbitrary time (eq. 10) is

$$P_{ON} = \mu T/(1 + \mu T). \tag{40}$$

Thus the longterm mean rate of occurrence of events (eq. 11) is

$$\nu = \mu/(1 + \mu T). \tag{41}$$

By introducing (39) into (16) and carrying out the indicated operations, one finds

$$P(0 \leq \theta \leq T) = \mu\exp(-\mu\theta) \tag{42}$$

$$P(T \leq \theta \leq 2T) = \mu\exp(-\mu\theta) + \mu^2(\theta-T)\exp(-\mu(\theta-T)) \tag{43}$$

$$P(2T \leq \theta \leq 3T) = \mu\exp(-\mu\theta) + \mu^2(\theta-T)\exp(-\mu(\theta-T)) + (\mu^3(\theta-2T)/2)\exp(-\mu(\theta-2T)). \tag{44}$$

The apparent generalization of this sequence,

$$P(\theta) = \mu\sum_{k=0}^{[\theta/T]}((\mu(\theta-kT))^k/k!)\exp(-\mu(\theta-kT)), \tag{45}$$

can be proved by induction using eq. (16). This form can be thought of as a generalization of the Poisson process wherein $P(\theta) = \mu$ everywhere. Indeed, when the events have vanishing duration, we retrieve the obvious result

$$\lim_{T\to 0} P(\theta) = \mu. \tag{46}$$

The limit of (45) as θ increases without bound is already known by prior reasoning (eq. 17) to be

$$\lim_{\theta\to\infty} P(\theta) = \nu = (1 - P_{ON})\mu = \mu/(1 + \mu T), \tag{47}$$

but it is difficult to derive this analytically. Straightforward numerical evaluation of (45), however, confirms that this limit obtains. Figure A-1 is a graph of $P(\theta)/\mu$-vs-θ/T for various values of P_{ON} (hence μT), plotted by evaluating (45) directly. For values of P_{ON} of 0.6 or less, the limit of (47) is achieved within a few periods, while for $P_{ON} = 0.8$, the function $P(\theta)$ is still oscillating substantially about the limit after four periods. This behavior is intuitively appealing; as the events grow more rare in occurrence, the probability of occurrence becomes less dependent upon the time of occurrence of any given event. But if the probability that an event is ongoing approaches unity, they occur with near certainty one after the other and the function $P(\theta)$ must degenerate toward a sequence of equally-spaced delta functions. Figure A-1 exhibits the near-constancy of $P(\theta)$ for $P_{ON} = 0.2$ and the approaching onset of the latter pathology at $P_{ON} = 0.8$.

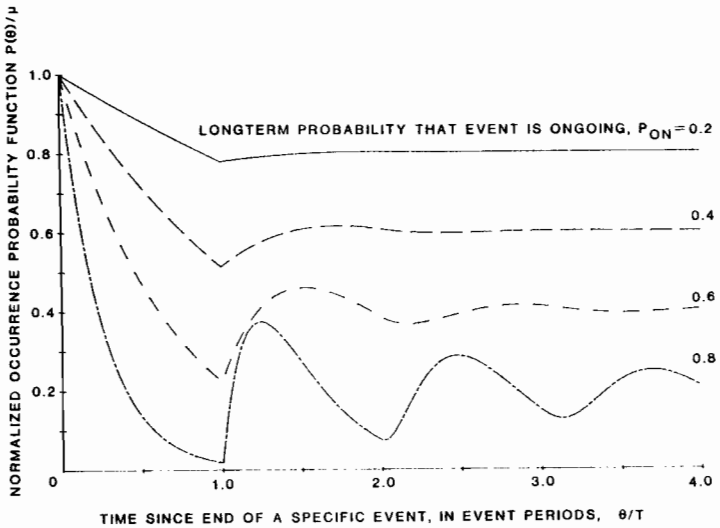

Figure A-1.--Probability density for event occurrence following termination of a given event. The asymptote for each curve is 1-P_{ON}, since the plotted variable, P(θ)/μ, is normalized by the mean occurrence rate (Equation 45).

One may further note that each term in the sum of eq. (45) is the probability of observing exactly k events in the total event-occurrence time span θ-kT when the events occur at random with constant mean rate μ; i.e., the number of events, k, is Poisson distributed[1] with mean μ(θ-kT).

Evaluation of Power Spectra

Using eq. (45) in the integral in eq. (38) gives the power spectral density of the process described. To obtain a closed form expression, we must evaluate the integral I:

$$I = \int_0^\infty P(\tau)\cos(\omega\tau+\omega T)d\tau = \sum_{n=0}^{\infty}\int_{nT}^{(n+1)T} P(nT\leq\tau\leq(n+1)T)\cos(\omega\tau+\omega T)d\tau \qquad (48)$$

$$= \sum_{n=0}^{\infty}\sum_{k=0}^{n}\int_{nT}^{(n+1)T} \mu\frac{(\mu(\tau-kT))^k}{k!}\cos(\omega\tau+\omega T)\exp(-\mu(\tau-kT))d\tau \qquad (49)$$

in which the circular frequency ω = 2πn is used. Changing the integration variable to μ(τ - kT) = x and interchanging the order of the two sums eliminates one summation and simplifies the result to

$$I = \sum_{k=0}^{\infty}\frac{1}{k!}\int_0^\infty x^k\cos((k+1)\omega T + \omega x/\mu)\exp(-x)dx. \qquad (50)$$

---

[1]An alternative derivation of (45) can be based on this fact, using the recursion (16) to evolve the probability $P_n(\theta)$ that an event starts at θ,θ+dθ given the occurrence of n intervening events. Analyst Fred Bratten (USDA Forest Service, PSW-Riverside) commended this approach to the author.

Expressing the cosine in imaginary exponent form and interchanging the order of summation and integration gives the form

$$I = \frac{1}{2}\int_0^\infty \exp(-x)[\exp(i(\omega T + \omega x/\mu) + x\exp(i\omega T)) + \exp(-i(\omega T + \omega x/\mu) + x\exp(-i\omega T))]dx \quad (51)$$

where i is the unit imaginary.

In (51) each term is absolutely convergent, and the results are simple complex fractions

$$I = -\frac{1}{2}[(1 - (1 - i\omega/\mu)\exp(-i\omega T))^{-1} + (1 - (1 + i\omega/\mu)\exp(i\omega T))^{-1}]. \quad (52)$$

Combining terms and simplifying gives the compact result

$$I = -\frac{1 - \cos(\omega T) + (\omega/\mu)\sin(\omega T)}{2(1-\cos(\omega T)+(\omega/\mu)\sin(\omega T))+(\omega/\mu)^2}. \quad (53)$$

Since the factor in (38) involves 1+2I, the result is even simpler due to cancellation of terms, leaving, finally

$$\frac{S_x(n)}{P_{ON}A^2T} = \frac{32\ \sin^4(\frac{\omega T}{4})}{(\omega T + \mu T\sin(\omega T))^2 + (2\mu T\sin^2(\frac{\omega T}{2}))^2}. \quad (54)$$

The limiting forms of (54) have the correct behavior, as can be verified by direct computation. When the events become exceedingly rare, the autocorrelation function has a nonzero value only over the period of a single event, leading to

$$\lim_{\mu T\to 0} \frac{S_x(n)}{P_{ON}A^2T} = \frac{2\ \sin^4(\frac{\omega T}{4})}{(\omega T/4)^2}. \quad (55)$$

When the opposite condition obtains, so the square wave becomes a continuous steady signal, the power spectrum must degenerate to series of delta functions at odd multiples of the period T. The form of (54) does so in that

$$\lim_{\mu T\to\infty} \frac{S_x(n)}{P_{ON}A^2T} = \frac{2}{(\mu T)^2}\tan^2(\frac{\omega T}{4}), \quad (56)$$

which vanishes everywhere except for being indeterminate at $n=\omega/2\pi=(2M+1)/T$, where M is an integer.

The power spectral density as expressed by (54) is graphed in the text for various values of the parameter μT, expressed in terms of P_{ON}. These figures illustrate that the shape of the spectrum is quite insensitive to the value of P_{ON} unless $P_{ON} > 0.8$. This is consistent with the generally benign behavior of the probability function $P(\theta)$ for $P_{ON} < 0.8$. In other words, most of the variation of $S_x(n)$ with frequency is contained in the dependence on ωT expressed by the limiting form for $P_{ON} \to 0$ unless $P_{ON} > 0.8$. The amplitude factor $P_{ON}A^2T$ and the frequency at which the first maximum of (55) occurs ($nT \doteq 0.742$) suffice to determine the greatest part of the whole spectrum for modest values of P_{ON}. This fact affords considerable simplification in the application of the derived power spectrum intended here.

ERRATA

Albini, Frank A.
"Potential spotting distance from wind-driven surface fires" USDA Forest Service Research Paper INT-309, April 1983, 27 p.

Table 3 (p. 11), Table 4 (p. 12), and numerical examples, pp. 13-15 contain numerical inaccuracies. The nature of the errors is such as to cause underestimation of maximum firebrand heights by approximately 70 percent. These data are superseded by those to be found in:

Chase, Carolyn H.
"Spotting distance from wind-driven surface fires--extensions of equations for pocket calculators" USDA Forest Service Research Note INT-346, 1984. The Chase publication will be available from the Intermountain Forest and Range Experiment Station in November, 1984.

# #

Albini, Frank A. Potential spotting distance from wind-driven surface fires. Res. Pap. INT-309. Ogden, UT: U.S. Department of Agriculture, Forest Service, Intermountain Forest and Range Experiment Station; 1983. 27p.

Equations are presented by which to calculate the maximum firebrand particle lofting height from wind-driven line fires in surface fuels. Variables used are the fuel type, described as one of twelve stylized models used for fire behavior prediction, the fire intensity, and the mean windspeed at 10 m height. Using the maximum particle lofting height, downwind drift of the firebrand particle during lofting and maximum spot fire distance are calculable from equations presented here and published elsewhere. The model upon which the equations are based assumes that the particle is transported upward by a two-dimensional thermal. Such thermals are assumed to be generated by variations of fire intensity with time. Both assumptions are speculative and probably not subject to direct test, so the model is considered tentative. Field test of the model predictions will reveal whether or not it provides useful estimates of spot fire distance.

KEYWORDS: spot fires, spotting, firebrands

☆ U.S. GOVERNMENT PRINTING OFFICE: 1983—676-032/51 REGION No. 8

The Intermountain Station, headquartered in Ogden, Utah, is one of eight regional experiment stations charged with providing scientific knowledge to help resource managers meet human needs and protect forest and range ecosystems.

The Intermountain Station includes the States of Montana, Idaho, Utah, Nevada, and western Wyoming. About 231 million acres, or 85 percent, of the land area in the Station territory are classified as forest and rangeland. These lands include grasslands, deserts, shrublands, alpine areas, and well-stocked forests. They supply fiber for forest industries; minerals for energy and industrial development; and water for domestic and industrial consumption. They also provide recreation opportunities for millions of visitors each year.

Field programs and research work units of the Station are maintained in:

Boise, Idaho

Bozeman, Montana (in cooperation with Montana State University)

Logan, Utah (in cooperation with Utah State University)

Missoula, Montana (in cooperation with the University of Montana)

Moscow, Idaho (in cooperation with the University of Idaho)

Provo, Utah (in cooperation with Brigham Young University)

Reno, Nevada (in cooperation with the University of Nevada)